TNL

Full Band Simulator
User Manual

Material Characterization simulation Software

Tech Next Lab (P) Ltd
Building No. #417/22/A, Niwaz Ganj,
Near Napier Road Park, Lucknow - 226 003, (U.P.), India,
Tel: **(+91) 522 404 1565**,
Web: **www.technextlab.com**

1st March, 2022

Notice

The information contained in this document is subject to change without notice.

Tech Next Lab (P) Ltd is not liable for any kind of warranty related to this material. The limited warranty extends ONLY for warranty of fitness for a purpose of particular requirement.

Tech Next Lab (P) Ltd shall not be held liable for typographical errors contained in the material. The users of this manual will be solely responsible for use of this manual, for incidental or consequential damages in connection with the furnishing, and performance.

The family of unmatched innovative simulators includes;

1. **TNL Framework** *(A GUI enabled control frame accommodating the Family of TNL Simulators)*
2. **TNL-EpiGrow Simulator** *(Epitaxial Growth through MBE/CVD/MOCVD reactors processes)*
3. **TNL-FB Simulator** *(Electronic Full Band Structure)***,**
4. **TNL-EM** *(Electron Mobility simulator)*
5. **TNL-TS Simulator** *(THz Spectroscopy with Ultrafast Carrier Dynamics Predictions)*
6. **TNL-PD Simulator** *(Particle based Device Simulator)*
7. **StrViewer, TNLPlot** (Graphical and Structural viewers)

Additional information is provided at:

http://www.technextlab.com

TNL

Contents

TNL

Blank Page

CHAPTER 1
INTRODUCTION

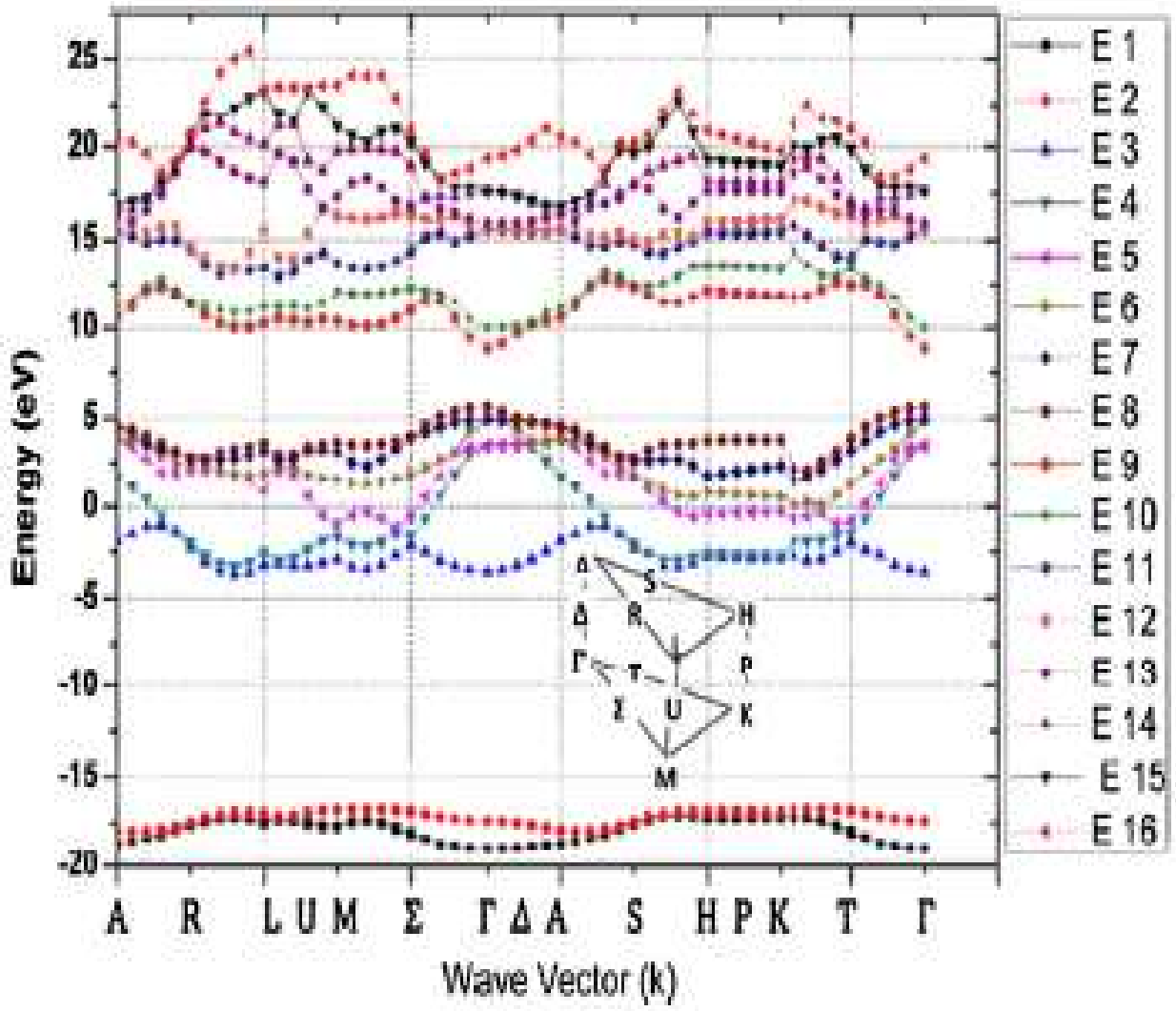

TNL

1.1 Need of FullBand Simulator

On the planet, only four of the ninety two naturally occurring elements have been exploited significantly which have altered the way of the lives. The industrial revolution without iron (Fe), modern medicine development without the understanding and utilizations of carbon (C), or the cold war without the Uranium (U) is impossible. Similarly, the modern human life could not be imagined without silicon (Si). Most of the modern electronic devices contain silicon technology based integrated circuits. The silicon is the back bone of the modern electronics industry. However due to its indirect band gap property which make it unsuitable for the use of optoelectronic applications. Therefore new material systems involving combination of the groups III-V elements, groups II-VI elements, group IV-IV elements are now being investigated. The growth techniques such as chemical vapor deposition (CVD), Metallo-organic vapour phase epitaxy MOVPE and Molecular Beam Epitaxy (MBE) processes made it possible to control the growth even upto a monolayer accuracy (sub nanometer) of different semiconductor compounds. Thus in addition to the bewildering combination of semiconductor alloys, the electronic properties can also be modified.

The prediction of the material properties through theoretical model of semiconductor materials or devices initiates from the dispersion relation (E-k). The energy wave (E-k) relation provides valuable microscopic level information regarding electronic band structure and the macroscopic properties. The knowledge of the bandstructure is the essential requirement in a many stage calculation with the increasing complexity of semiconductor systems. The advanced semiconductor materials, including combination of groups IV & IV (Cubic) or, groups III & V and groups II & VI materials in Zincblende and Wurtzite phases has introduced new challenges in the area of electronic transport modeling for device applications. Wide band materials have poses extra challenges in terms of large number of electronic bands with a small energy distance between each band in significant part of Brillouin zone allowing significant band-to-band tunneling or impact ionization mechanisms at high applied electric fields application. On the other hand, low dimensional semiconductor microstructures (nanometer scale thickness) pose extra challenge in terms of the quantum confinement effects. The essential requirement for full band Monte Carlo carrier transport simulation is information of different physical parameters on the full electronic band for real transport of carrier's on different bands and valleys.

The important role of the band structure has led to a large number of techniques for its description. These vary from the simplest models (assuming parabolic bands) to highly complex models (ab-initio, self-consistent, many body effects etc.). They have varying degrees of applicability and complexity reflecting the wide range of calculations for which band structures are required. Electronic band structure calculation methods can be grouped into two general categories [1].

The first category consists of *ab initio* methods, such as Hartree-Fock or Density Functional Theory (DFT), which calculate the electronic structure from first principles. In

general, these methods utilize a variational approach to calculate the ground state energy of a many-body system, where the system is defined at the atomic level. The original calculations were performed on systems containing a few atoms. Today, calculations are performed using approximately 1000 atoms but these methods are still computationally expensive, sometimes requiring massively parallel computers.

The second category consists of empirical methods in contrast to ab initio approaches, such as the Orthogonalized Plane Wave (OPW) [2], tight-binding [3] (also known as the Linear Combination of Atomic Orbitals (LCAO) method), the $k \cdot p$ method [4], and the local [5], or the non-local [6] empirical pseudopotential method (EPM).

The EPM has advantage of being a full k space representation while being defined with only a handful of adjustable parameters. These methods involve empirical parameters to fit experimental data such as the band-to-band transitions at specific high-symmetry points derived from optical absorption experiments. The appeal of these methods is that the electronic structure can be calculated by solving a one-electron Schrödinger wave equation (SWE). Thus, empirical methods are computationally less expensive than ab initio calculations and provide a relatively easy means of generating the electronic band structure with accuracy. The main advantage of using pseudopotentials is that only valence electrons have to be considered. The core electrons are treated as if they are frozen in an atomic-like configuration.

The main feature of TNL-FB (Full Band) simulator, its ability to analyze the full electronic band structures by just inputting the lattice parameter, crystal orientation and film thickness of the zincblende and wurtzite materials The impact of orientation and thickness of the thin film on the bandgap, demonstrate the appropriate atomistic physics based effects. The TNL-FB (Full Band) simulator is equipped with graphical user interface (GUI) enabled capabilities on the windows platform. The various physical parameters e.g. electron effective masses, density of states (DOS), group velocity of the corresponding anisotropic band structure etc at high symmetry points can be extracted using TNL-FB (Full Band) simulator. The calculated parameters can be calibrated against reported existing experimental data and can be used in the interpretation of experiments and for numerical simulation purposes. It provides flexibility to choose user defined materials lattice parameters, pseudopotentials and analyze the full electronic band structures over computer. There is also flexibilities to incorporate user defined material in the TNL-FB (Full Band) simulator.

1.2 TNL-FB (FullBand) Simulator Overview

TNL-FB Simulator is powerful tool to simulate full electronic band structure with various basic parameters extraction capabilities e.g. electronic properties of the IV-IV, III-V and II-VI groups materials. The full electronic band structures of the elemental, binary, ternary and quaternary semiconductor materials in zincblende (ZB) and wurtzite (WZ) phase symmetries can be simulated. The simulator uses only lattice parameters either obtained from XRD studies or through simulated lattice parameter from TNL-EpiGrow simulator. By default database for the elemental and binary semiconductors inbuilt, for ternary alloys are material parameters are extracted through interpolation of the parameters of the binary alloys. The thin film structure quality plays a significant role in deciding the optical band gap values. The simulator includes virtual crystal approximation (VCA) techniques to estimate the impact of alloy disorder effect. The impact of intrinsic & extrinsic dopings and the polycrystalline planes in thin film samples on the band gap parameter can be analyzed in terms of the internal structure factor, u. It is assumed that the lattice parameter contains information about strain associated with each monocrystalline layer of thin film. TNL-FB simulator has capabilities for analyzing the lattice disorder generated by the formation of various defects and polycrystalline planes in the thin films. The impact of crystal orientation and film thickness is also included in the TNL-FB Simulator.

1.3 Features

TNL-FB (Full Band) software is a graphical user interface (GUI) based software tool which run on the Windows platform with full capabilities.

- Full Electronic band structure of the group IV, III-V and II-VI binary, ternary and quaternary compounds
- Zincblende and Wurtzite phase symmetries
- Lattice constants of binary materials have been used to determine the lattice constant of the ternary alloy through interpolation
- Virtual crystal approximation (VCA) included
- Alloy disorder due to dopants
- Strain and Deformation potential mapping
- Semi-empirical disorder contribution included
- Different energy valleys
- Local atomic pseudopotentials
- Non-local pseudopotential included
- Spin-orbit interaction included
- Extraction of Full Band Structures, Reflectivity Spectra, Electronic Densities of States, etc.

1.4 *Comprehensive details of Models and Key words*

TNL-FB (Full Band) simulator includes a comprehensive set of models and key words, including;

- Schrodinger Equation
- Reciprocal lattice
- Miller Indices
- Brilloulin Zone
- Virtual Crystal Approximation
- Alloy Disorder Effect
- Doping
- Strain
- Hamiltonian
- Eigen function and eigenvalue
- Wavevector
- Dispersion Relation
- Born Oppenheimer approximation
- Pseudopotential
- Symmetric and Asymmetric
- Spin-Orbit Coupling
- Zincblende
- Wurtzite
- Rocksalt
- Internal Structure Parameter

1.5 Integrated Capabilities

TNL- FB (Full Band) simulator works well with other family of TNL simulator software from Tech Next Lab. For example, FBS

- Runs in the TNL Framework interactive run-time environment equipped with GUI capabilities.
- Interfaced to TNL-EM simulator (Electron Mobility), TNL-TS simulator (THz Spectroscopy), TNL-PD simulator (Particle device) and TNLPlot, an interactive graphics and analysis package.
- Various binary and ternary materials examples are inbuilt.
- Various material data base for group IV, III-V and II-VI semiconductors inbuilt.
- Flexibility to accommodate user define materials and properties.

1.6 Numerical Implementation

TNL- FB simulator uses powerful numerical techniques, including:

- Accurate and reliable Schrodinger solution techniques.
- Crystal orientation dependence
- Lattice parameters (a, c)
- Symmetric Pseudopotential (V_s)
- Symmetric Pseudopotential (V_a)
- Internal Structure Parameter (u)
- Thin film thickness dependence
- Virtual crystal approximation for ternary and quaternary alloys
- Alloy disorder computational flexibility
- Solution of one-electron Schrodinger equation resulting from the variational method by using a base of plane wave
- Many body problem
- No convergence issues

1.7 Benefits can be realized

- Pseudopotential database available for calibration
- Flexibilities to use User defined pseudopotentials
- Binary (GaN, GaAs etc.) and ternary (AlGaN, InGaAs etc.) material database
- Flexibility to input User defined lattice constant of thin-film
- Full Electronic Energy Band extraction
- Extraction of Velocity of carriers in different energy states
- Extraction of Effective Mass of carriers on Full Electronic Band Structure
- Parabolic & Nonparabolic bands coefficient extraction
- Density of state (DOS) calculation
- Ability to deal with different cubic, Zincblende & Wurtzite alloys
- Carrier's position & energy on different Energy levels on Full Band Structure
- User define materials can be inputted
- User defined crystal symmetries can be inputted

Chapter 2
Start using FullBand Simulator

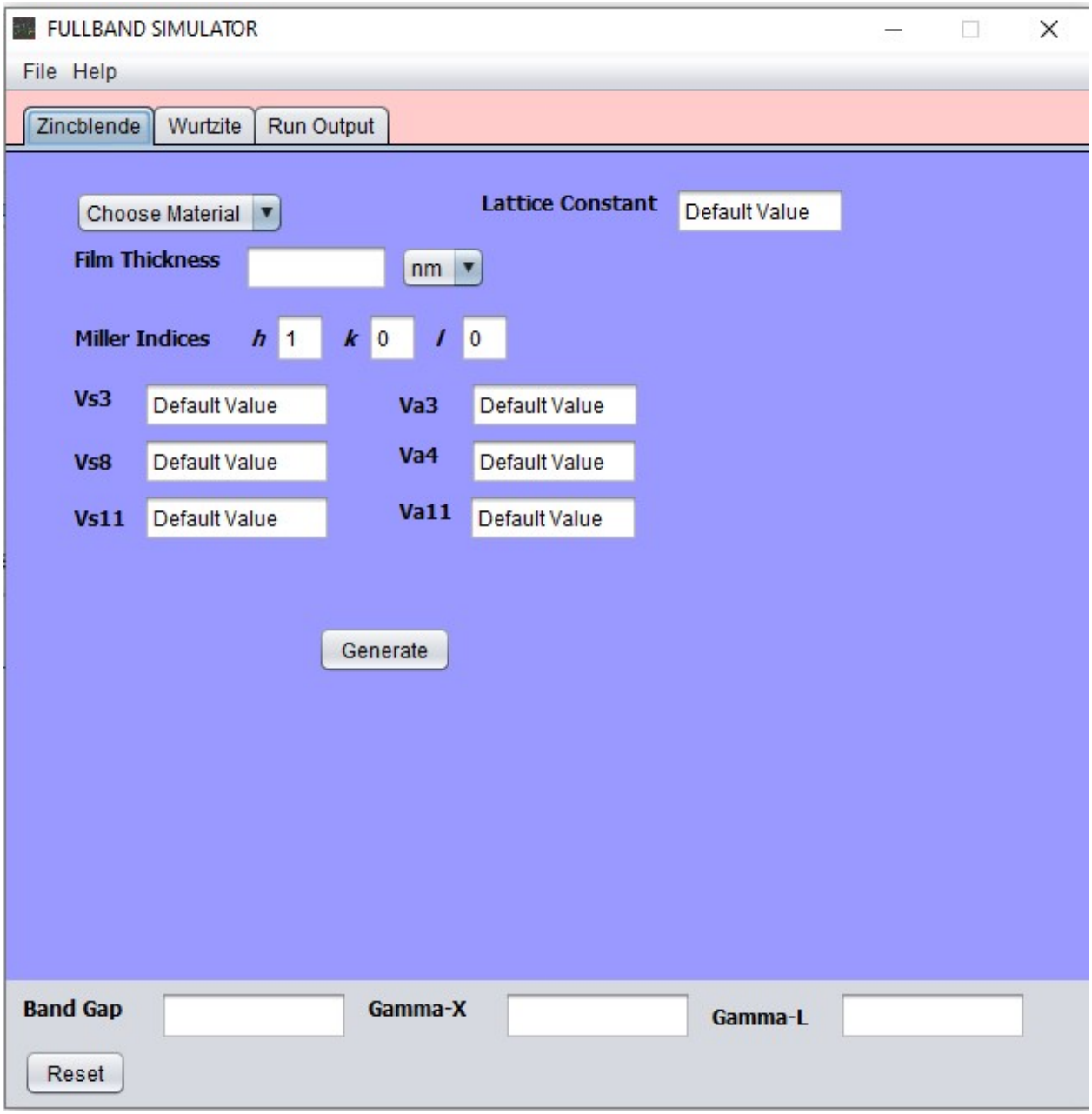

TNL

2.1 Summary

TNL-FB (FullBand) simulator is a purely physics based simulator capable to simulate full electronic band structure of elemental and compound semiconductor materials. A well established empirical pseudopotential method is used as a direct simulation of dispersion relation for the given lattice based on lattice parameters and pseudopotentials. The TNL-FB (FullBand) simulator is use to extract various physical information associated with full band structure which is demonstrated in this tutorial. The solution of Schrodinger equation under the Born-Oppenheimer approximation is carried out through orthogonal plane wave method for the accurate prediction of the band gap and different energies, effective mass on different valley, group velocity of the carrier's in different valley, density of states (DOS), different energies values of different bands, information regarding deformation potential, low & high permittivity of the material etc.

The TNL-FB (FullBand) simulator paves way for the calculations of electronic band structure parameters are important prerequisite for the carrier transportation on the full band structure. It can work as standalone tool as well as in interfaced environment through conjunction with TNL-EM simulator, TNL-TS simulator and TNL-PD (Particle Device) simulator. This chapter will describe the step by step execution of TNL-FB (FullBand) simulator effectively. Being as GUI based simulator, it is user friendly.

2.1.1 The Graphical User Interface

The graphical user interface (GUI) capabilities of TNL-FB (FullBand) simulator extend a convenient and comfortable approach to users for extracting input conditions and physical parameters required for the carriers transportation on the full electronic band structure. Users need to choose the appropriate material from database and either including database parameters or input their own lattice constant and pseudopotentials at the appropriate locations to initiate the simulation. The run output window allows users to check the initial data inputted by them. The simulation running information is also printed in the run output window.

2.1.2 Start Using TNL-FB (FullBand) Simulator

The TNL-FB (FullBand) simulator is integrated inside the TNL Framework and takes advantage of the framework environment.

Users need to open TNL framework and double click on Full Energy Band Simulator as shown in the below figure:

A new frame of TNL-FB (Full Band) simulator window will be open as shown below: It contains three sub windows: Zincblende, Wurtzite and Run Output options;

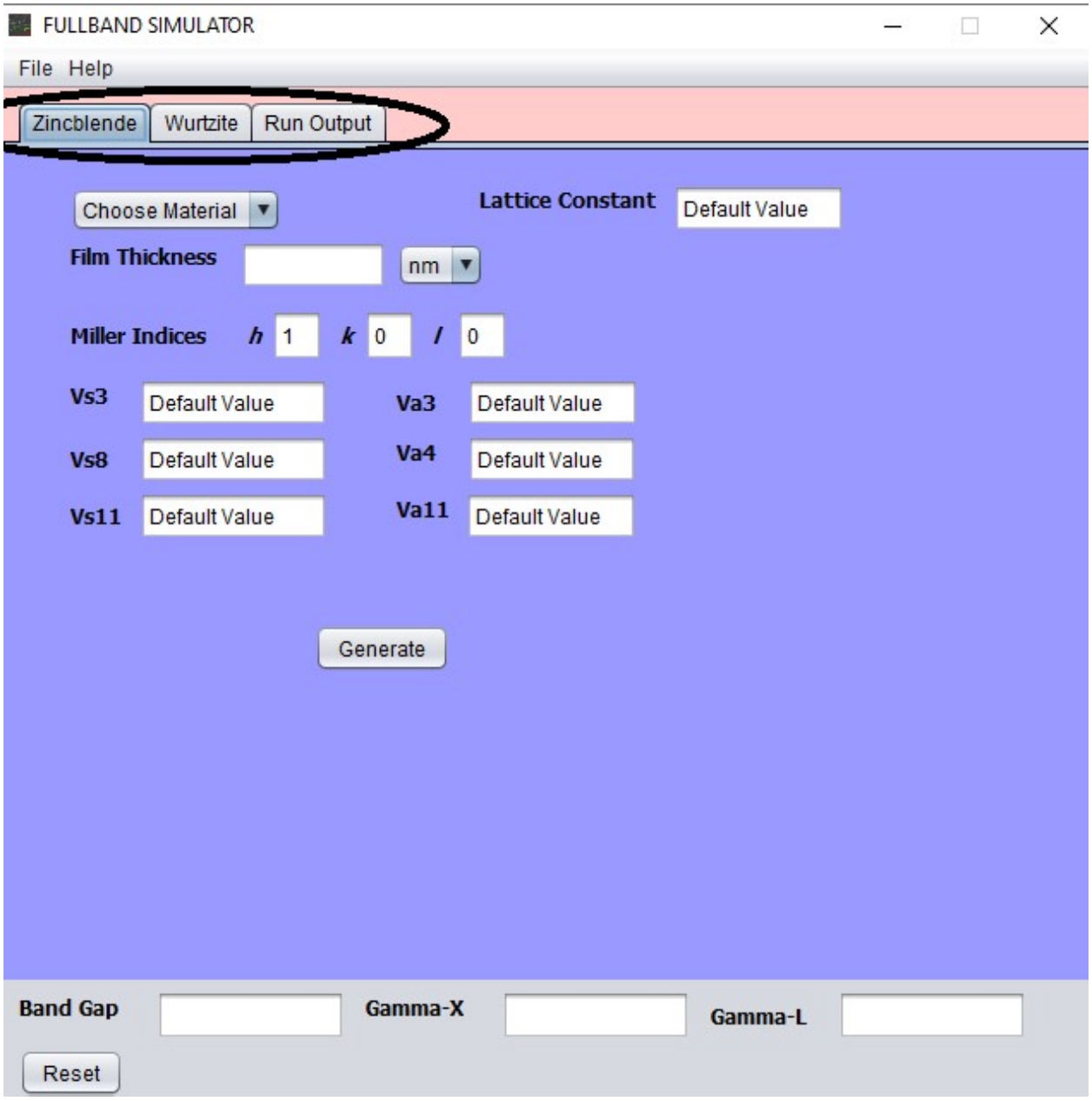

2.1.3 Diamond & Zincblende Stuctures

After clicking on Zincblende option, simulator will load zincblende material database as shown below;

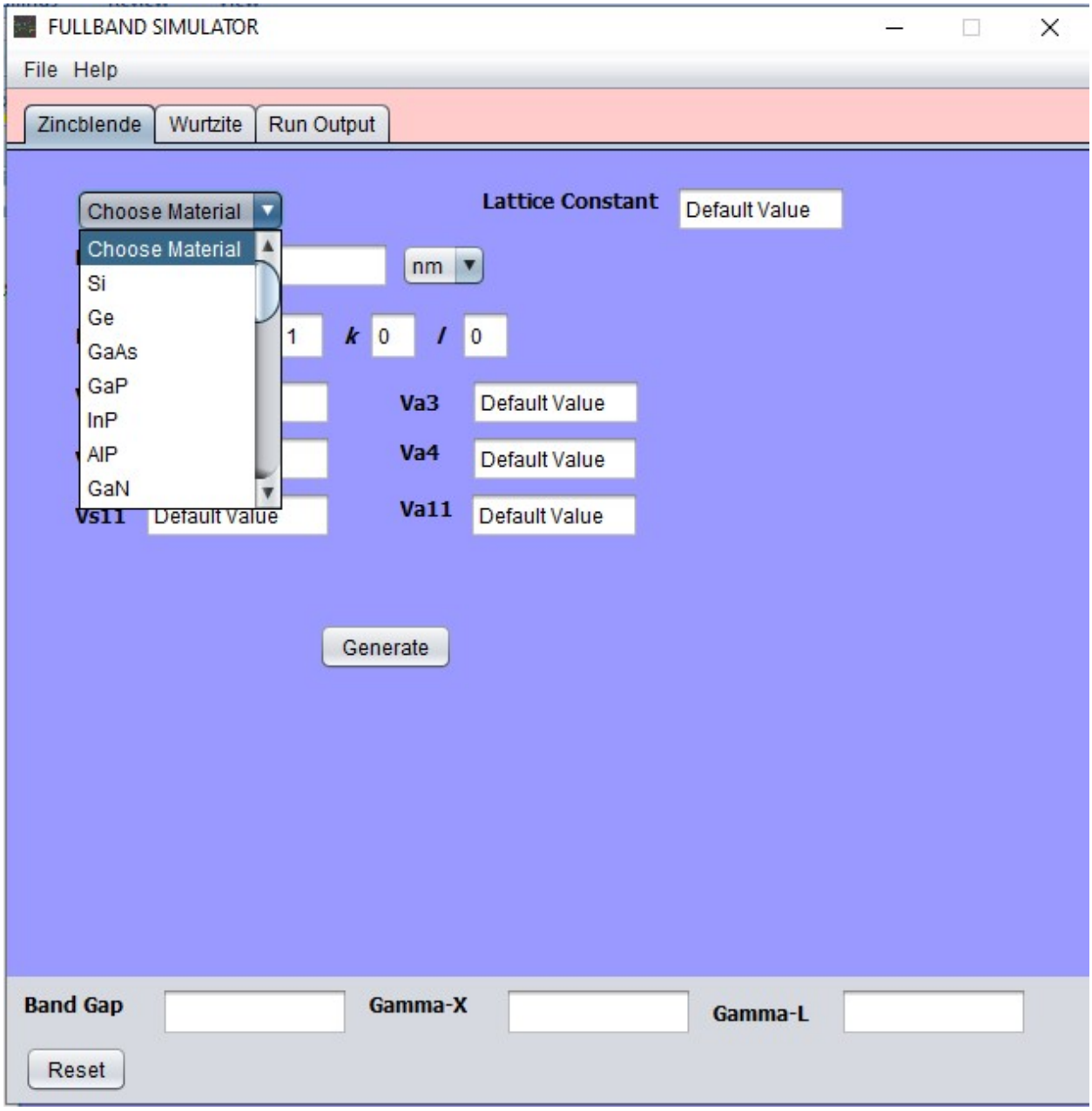

Most of the zincblende phase elemental, binary and ternary materials are inbuilt in the TNL material database. After choosing the material, the lattice constants and pseudopotentials will shown at appropriate locations.

The elemental semiconductors the asymmetric pseudopotential V_a's values are zero by default. It may be understood in terms of elemental crystal structure symmetry.

In case, user chooses compound binary or ternary material, the asymmetric pseudopotential V_a's values will not be zero as the crystal structure depends on combination of two atoms which may not be symmetrical and asymmetry arises due to atom radius, bond length and bond angle etc.

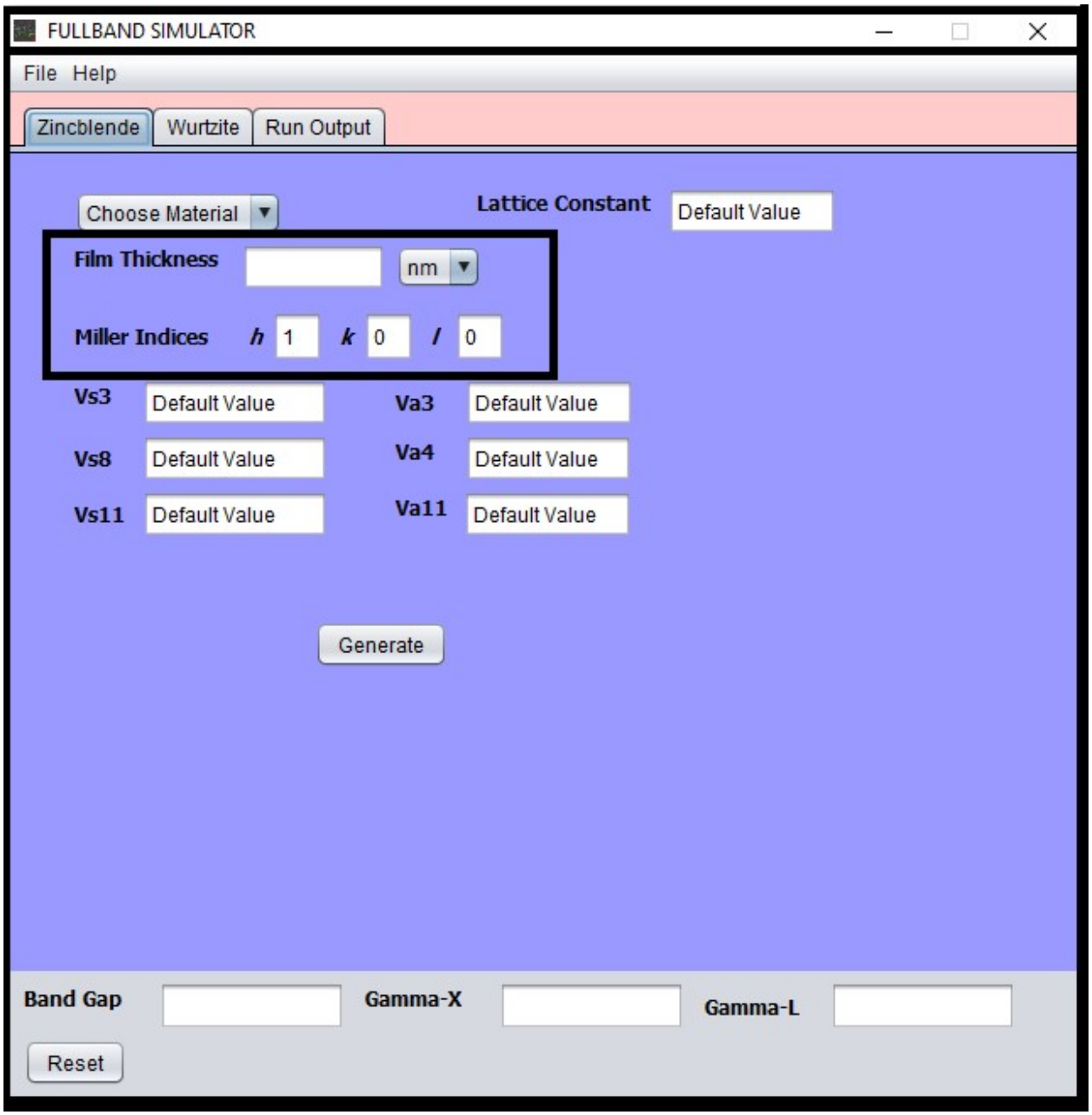

After choosing material from TNL material database, Users need to fill the value of thickness of the film and the miller indices i.e. orientation of the film for which full band structure is simulated at the ensquared location.

After filling these values, click on Generate button to invoke the full band simulation. It will ask to save the output data files.

Users may choose appropriate location in their computer for saving the output data files. After saving data files users may click on Run Ouput subwindow to check whether the run output is coming means simulation is running or not. In the run output window the message will be displayed; Simulation Successfully Completed!!! means simulation is finished.

The value of Bandgap means difference of conduction band minima and valance band maxima at Γ valley will be automatically displayed in the lower portion of FullBand Frame at the location of Band Gap values. User may check the Full Band Structure by invoking the TNLPlot and call the output file saved by user at the initial step.

TNLPlot window will be opened, user need to click on File option and load the output data file saved by user before starting the simulation. The full band structure can be plotted in TNLPlot window. The x-axis represents the wave vector ‘k’ and y-axis represents the Energy (E). In the case of zinc blende materials, the different valley positions can be calculated from the green encircled positions as shown below:

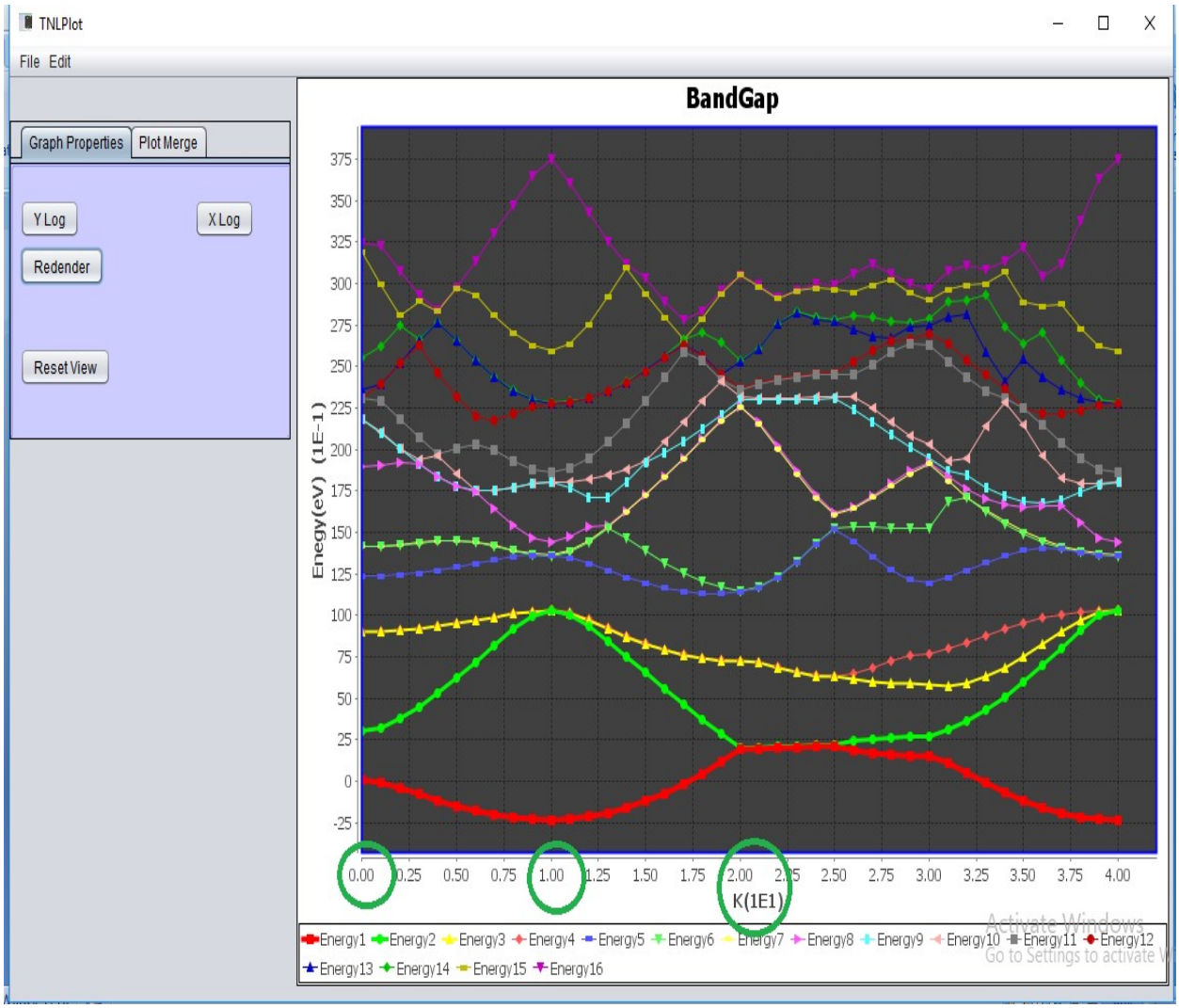

For zinc blende materials, the different symmetry points in form of valley locations at the Brillion zone of the solid are given.

Starting with the L valley is located at k=0 at the x-axis, the matrix for energy values with wave vector k has been solved at linearly spaced intervals between high symmetry points as described below.

$$\mathbf{L}=\frac{2\pi}{a}\left(\frac{1}{2},\ \frac{1}{2},\ \frac{1}{2}\right)\rightarrow\ \mathbf{\Gamma}=\frac{2\pi}{a}(0,0,0)\rightarrow\mathbf{X}=\frac{2\pi}{a}(1,\ 0,\ 0)\rightarrow\mathbf{W}=\frac{2\pi}{a}\left(1,\ \frac{1}{2},0\right)$$

$$\rightarrow\mathbf{K}=\frac{2\pi}{a}\left(\frac{3}{4},\ \frac{3}{4},\ 0\right)\rightarrow\mathbf{Gamma}=\frac{2\pi}{a}(0,0,0)$$

These symmetry points are also printed in the run output window showing k_x, k_y and k_z values. User may see the run output data and count & check different k_x, k_y and k_z values.

For the Zincblende materials, the wave vector k start with zero and ends with maximum value k=40.

At k=0 showing L valley with k_x=0.5, k_y=0.5 and k_z=0.5,

At k=10, the curve shows the Gamma valley (with k_x=0.0, k_y=0.0 and k_z=0.0),

At k=20, the curve shows the X valley (with k_x=1.0, k_y=0.0 and k_z=0.0),

At k=25, the curve shows the W valley (with k_x=1.0, k_y=0.5 and k_z=0.0),

At k=30, the curve shows the K valley (with k_x=0.75, k_y=0.75 and k_z=0.0),

At k=40, the curve again shows the Γ valley (with k_x=0.0, k_y=0.0 and k_z=0.0),

For ease of viewing, only the lowest 15 (out of 125) energy eigenvalues with respect to wave vector are plotted at each symmetry point while output data file contain all the eigenvalues with replication of same valleys for unit cell.

For more details user need to go through chapter 3 of this manual for better understanding of physics applied for simulation of full band structure.

2.1.4 Wurtzite materials

Most of the standard wurtzite phase based compound binary and ternary materials are already provided in TNL material database with the software. The standard lattice constants and pseudopotentials have been inbuilt in TNL material database.

In analogy with the zinc-blende phase materials, the wurtzite materials can be constructed by considering two interpenetrating lattices. However, in this case they are hexagonal close packed lattices instead of tertragonal. The nearest neighbors and next nearest neighbors are the same in the ideal wurtzite and zinc-blende structures. For the ideal wurtzite case, the lattice parameters are $\frac{c}{a} = 2\sqrt{\frac{6}{3}} = 1.633$, and $u = 3/8$. In case, the nearest neighbor distance is the same in the wurtzite and zinc-blende lattices, the lattice constants are related by the relation $a_z = \sqrt{2}.a_w$.

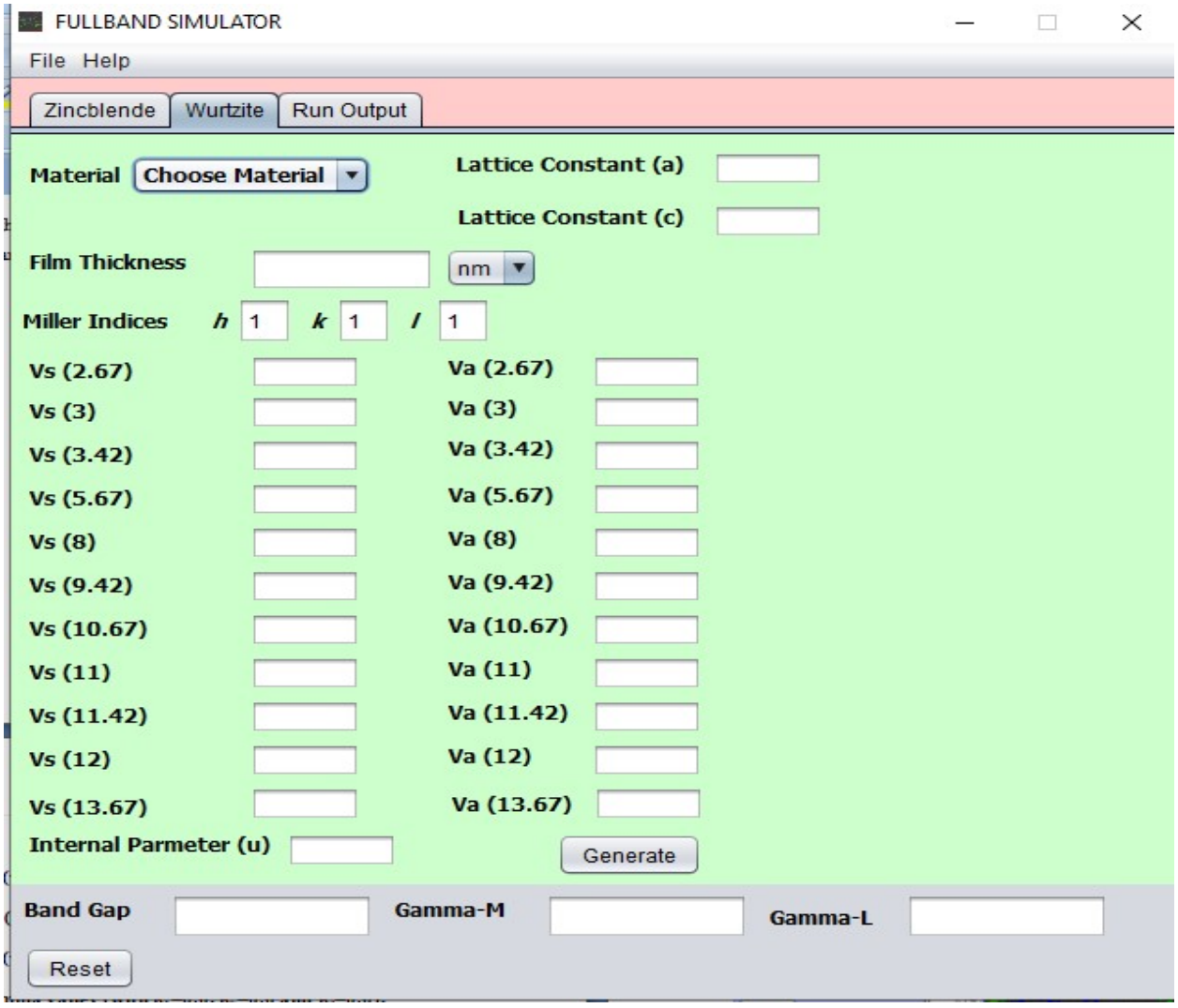

Users may note the difference in symmetry points of the wurtzite semiconductor materials, which are different for the cubic and zincblende materials symmetry points. The formalism used in simulating E-k diagram at hexagonal symmetry points for wurtzite semiconductor materials are given in the chapter 3, which demonstrate about the different symmetries and points in details.

For wurtzite, there are four atoms per unit cell as compare to two in case of zinc-blende. Since the volume per atom is the same, a given volume of reciprocal space for wurtzite crystal contains approximately twice as many reciprocal lattice points, which are given as;

$$\mathbf{A}=(0,\ 0,\ \tfrac{1}{2}) \rightarrow \mathbf{L}=(\tfrac{1}{2},0,\tfrac{1}{2}) \rightarrow \mathbf{M}=(\tfrac{1}{2},\ 0,\ 0) \rightarrow \mathbf{\Gamma}=(0,\ 0,0)$$

$$\rightarrow \mathbf{A}=(0,\ 0,\ \tfrac{1}{2}) \rightarrow \mathbf{H}=(\tfrac{1}{3},\ \tfrac{1}{3},\ \tfrac{1}{2}) \rightarrow \mathbf{K}=(\tfrac{1}{3},\tfrac{1}{3},0) \rightarrow \mathbf{\Gamma}=(0,0,0)$$

The wave vector k start with zero and ends with maximum value k=55 in case of wurtzite full band simulation.

At k=0 showing A valley with k_x=0.0, k_y=0.0 and k_z=0.5,

At k=10, the curve shows the L valley (with k_x=0.5, k_y=0.0 and k_z=0.5),

At k=15, the curve shows the M valley (with k_x=0.5, k_y=0.0 and k_z=0.0),

At k=25, the curve shows the Γ valley (with k_x=0.0, k_y=0.0 and k_z=0.0),

At k=30, the curve shows the A valley (with k_x=0.0, k_y=0.0 and k_z=0.5),

At k=40, the curve shows the H valley (with k_x=0.33, k_y=0.33 and k_z=0.5),

At k=45, the curve shows the K valley (with k_x=0.33, k_y=0.33 and k_z=0.0),

At k=55, the curve again shows the Γ valley (with k_x=0.0, k_y=0.0 and k_z=0.0),

The similar procedure need to be repeated (as for the case of zincblende materials) for the wurtzite semiconductors full band simulation is used for plotting the full electronic band structure.

The hexagonal material database is already inbuilt in the TNL material database and users have flexibilities to take user input values of lattice constants ‘a’ and ‘c’ and different symmetric and asymmetric pseudopotentials values.

The working of wurtzite full band simulator is same as described in the previous diamond and zincblende material simulation section.

The splitting of each band is showing spin-orbit coupling. According to Pauli's exclusion principle, two states are available in each orbital of each band. In wurtzite structure at normal pressure, there are four atoms in the unit cell, yielding eight valance bands. From the full band structure user may notice that bands 1 and 2 have a strong s-character whereas the rest of the bands have pronounced p-like character. In particular, bands 3 & 4 showing p_x-like, 5 & 6 showing p_y-like, and 7 & 8 showing p_z-like characters.

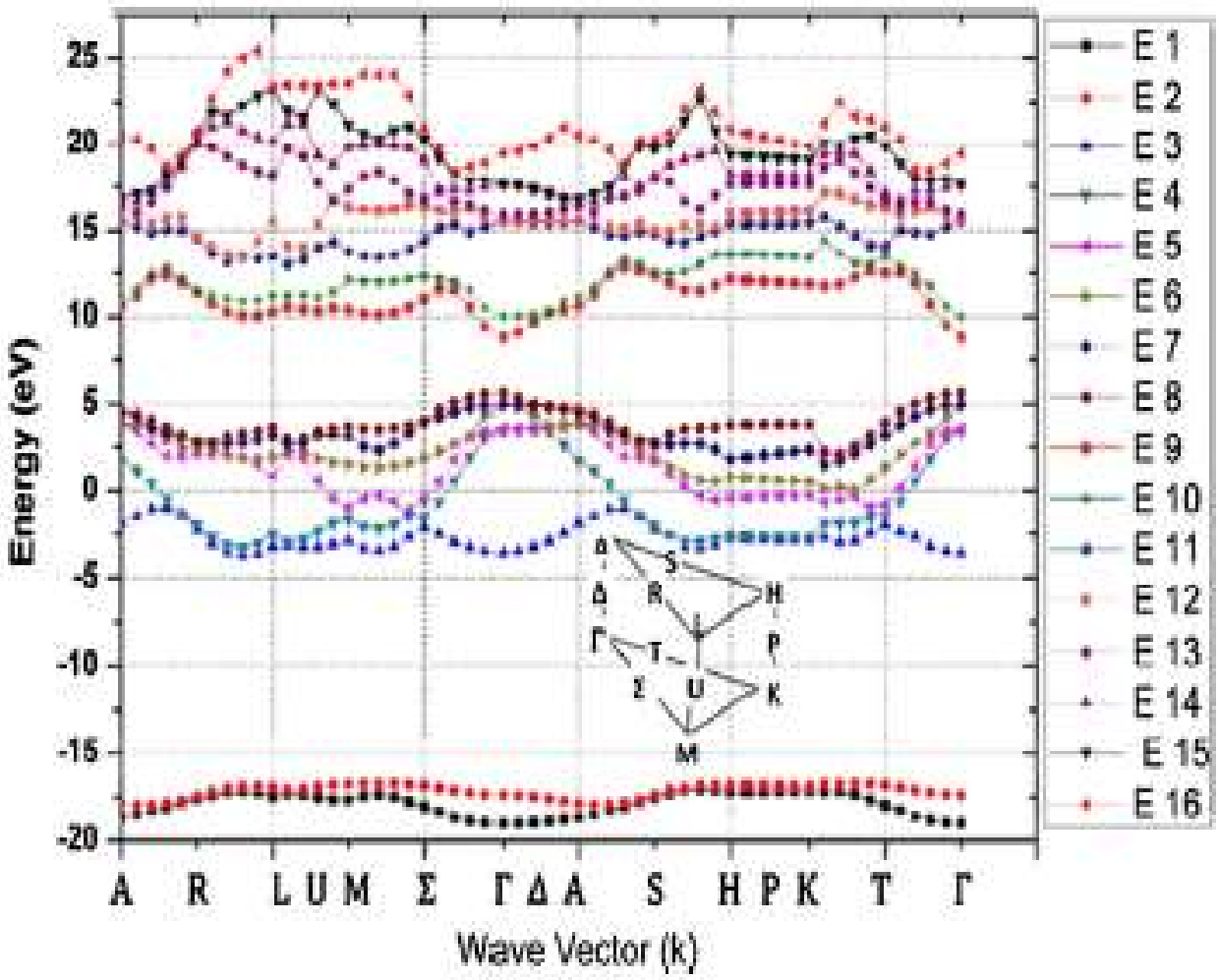

CHAPTER 3
Physics

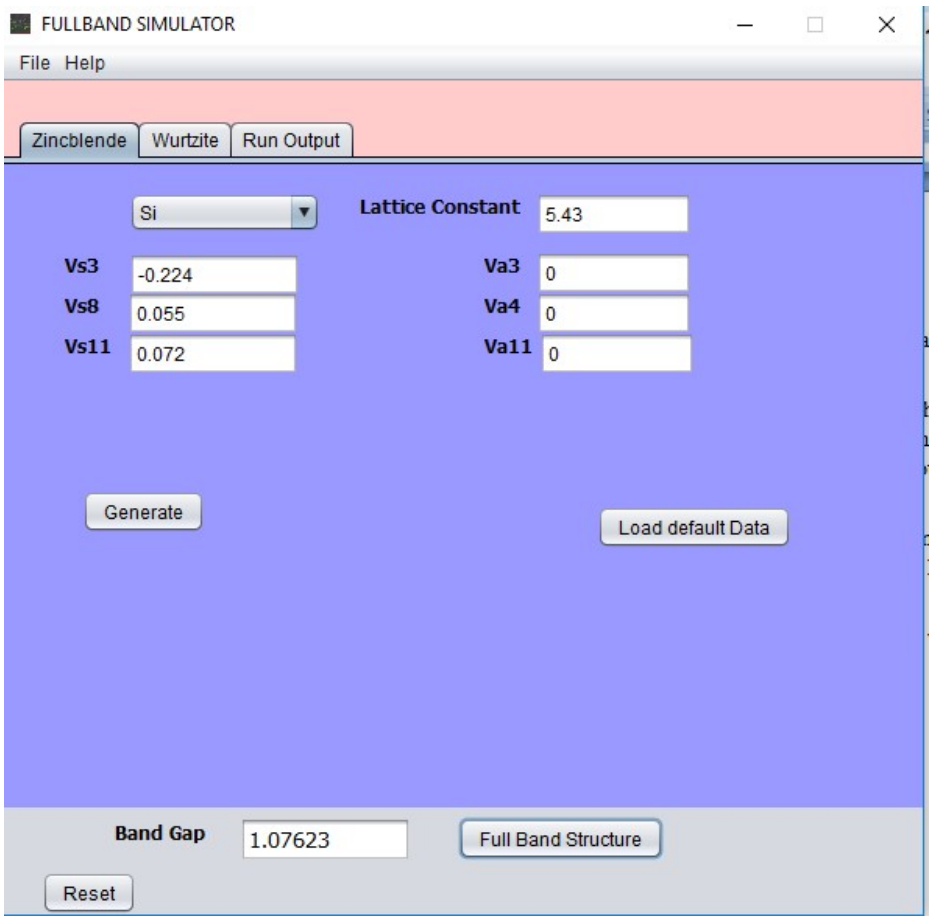

3.1 Introduction

The behavior of electrons and the existence of gaps in their electronic excitation spectra on the full energy band decides the conduction properties of the materials. The microscopic behavior of electrons in a solid is most conveniently specified in terms of the electronic band structure. Based on the electronic band structure of solids, the materials can be classified them into three groups on the basis of their bandgap values:

1. Metals
2. Semiconductors
3. Insulators

Our main emphasis is more about the semiconductor materials use for various bulk and nanometer device technologies. a semiconductor is usually defined rather loosely as a material with electrical resistivity lying in the range of 10^{-2} -10^{9} Ωcm. Alternatively, it can be defined as a material whose energy gap for electronic excitations lies between zero and about 4 electron volts (eV). This chapter includes the formalism used to simulate the band structure of the elemental and compound semiconductors and describe the fundamental physics used to analyze the electronic band structure for the most of common semiconductors, namely, Si, Ge, III–V and II-VI compounds.

Studies of semiconductor band structures have had a vast impact on our understanding of the fundamental electronic structures of solids. Although most device applications focus on the minimum semiconductor band gap, which is generally around 1 eV, solid-state physicists have been interested in a wider range of energy 1 Ry. Research on electronic structures in this range has led to tests of the theories of quantum mechanics, optics, and electromagnetism. The study of electronic transport requires knowledge about the energy levels that can be occupied by the electrons inside the solid. The band structure of a material can be used to predict its electrical and optical properties. Accurate knowledge of the band structure is important to predict the microscopic behavior of electrons in a solid. The semiconductor electronic band structure is the property which decides its specific device applications. The electronic band structure is the most efficient way to accurately estimate $E_n(k)$ and other parameters of semiconductors, and it can accurately predict electronic properties and work as a source of factual information about semiconductors.

There are several methods for prediction of the band structure of semiconductors is available. These methods can be grouped into two general categories.

The first method is based on an ab-initio approach which exploits either density functional theory (DFT) or Hartree–Fock techniques. Both techniques use first principles for the calculation of electronic band structures. In general, a variational technique is used to estimate the ground state energy of an atomic level of many body systems. A system containing less than 10,000 atoms can be calculated from these methods in a time which limits its applicability. On the other hand, these techniques are computationally very expensive.

The second method includes empirical methods which utilize various techniques, e.g., the orthogonalized plane wave, tight-binding, the k.p method, and the local or the non-local empirical pseudopotential method (EPM) to predict the electronic band structures. In these techniques, the experimental data are fitted by empirical parameters at specific high-symmetry points, such as band-to-band transitions derived from optical absorption experiments. In these methods, the electronic band structure is calculated by the solution of a one-electron Schrodinger wave equation, which makes the EPM approach computationally much-much cheaper compared to the ab-initio based methods. These techniques are relatively easy for the calculation of the electronic band structure in contrast to ab-initio methods. The main advantage of the EPM is that, in this technique, the core electrons are treated as frozen in an atomic-like configuration (Born–Oppenheimer approximation), and only valence electrons contribute to the calculation of the electronic band structure. The introduction of the pseudopotential method has become popular tools both for the investigation of electronic band structures of solids and for understanding the behavior of electrons inside crystals.

In TNL-FB (Full Band) simulator, the empirical pseudopotential method (EPM) is implemented to simulate $E_n(k)$ and other electronic properties of the semiconductors. The major virtue of this approach is that only the valence electrons need to be considered. The Born–Oppenheimer approximation in which cores are assumed to be frozen in an atomic-like configuration, and the valence electrons move in a net, weak one-electron potential. Computationally this is crucial because it means that the deep ion core electrons have been removed and a simple plane wave basis yields rapid convergence.

3.2 Translational Symmetry and Brillouin Zones

Brillouin zones are uniquely defined primitive cells in reciprocal space in crystalline materials and are the geometrical equivalent of Wigner-Seitz cells in real space. Physically, Brillouin zone boundaries represent Bragg planes which reflect (diffract) waves having particular wave vectors so that they cause constructive interference. To translate a geometric figure, i.e. to move it from one place to another without rotation is known as the translational symmetry. The most important symmetry of a crystal is defined through its invariance under specific translations. In addition to translational symmetry, most of the crystals also possess some rotational symmetry. The high degrees of rotational symmetry shown by most semiconductors are very useful in reduction of the complexity associated with the energy band structures calculations.

The particle movement in a periodic potential can be represented by its wavefunctions which is expressed in a form known as Bloch functions. The wave function is given as

$$\psi_{n,\mathbf{k}} = u_n(\mathbf{k})e^{i\mathbf{k}\cdot\mathbf{r}} \tag{3.1}$$

where k is the wavevector, and n represents the integer index corresponding to different solutions for a given wavevector. The periodic block function, $u_n(\mathbf{k})$, has the periodicity of the lattice potential and modulates the traveling wave solution associated with the electrons.

Suppose, equation (3.1) is one-dimensional and V(x) is a periodic function with the translational period equal to R. We will define a translation operator T_R as an operator whose effect on any function f(x) is given by

$$T_R f(x) = f(x + R) \tag{3.2}$$

and

$$\Phi_k(x) = u_k(x)e^{ikx} \tag{3.3}$$

By definition, when x changes to x+R, $\Phi_k(x)$ must change in the following way

$$T_R\Phi_k(x) = \Phi_k(x + R) = \Phi_k(x)e^{ikR} \tag{3.4}$$

The equation (3.4) shows that $\Phi_k(x)$ is an eigenfunction of T_R with the eigenvalue $\exp(ikR)$. Before going into details, let us know about the eigenvalue i.e. Hamiltonian and contribution of various electronic phenomenon inside solid.

The transportation of the ions in solid are slower due to its heavier mass and the vibrational frequencies are of order 10^{13}sec^{-1} as compared to the electronic motion frequencies of the order 10^{15}sec^{-1}. The solution of equation (3.1) can be expressed in terms of Hamiltonian under the Born-Oppenheimer approximation, which can be expressed as the sum of three terms:

$$\mathcal{H} = \mathcal{H}_{ions}(\boldsymbol{R_j}) + \mathcal{H}_{electrons}(\boldsymbol{r_i}, \boldsymbol{R_{j0}}) + \mathcal{H}_{ions-electro} \quad (\boldsymbol{r_i}, \boldsymbol{\delta R_{j0}}) \qquad (3.5)$$

Where, the Hamiltonian $\mathcal{H}_{\text{ions}}(R_j)$ represents the ionic motion under the influence of the ionic potentials plus the time-averaged adiabatic electronic potentials. $\mathcal{H}_{\text{electrons}}(r_i, R_{j0})$ is the Hamiltonian for the electrons with the ions frozen in their equilibrium positions R_{j0}, and $\mathcal{H}_{\text{ions}-\text{electr}}$ $(r_i, \delta R_{j0})$, describes the change in the electronic energy as a result of the displacements δR_{j0} of the ions from their equilibrium positions. $\mathcal{H}_{\text{ions}-\text{elect}}$ is known as the electron–phonon interaction and is responsible for electrical resistance in reasonably pure semiconductors at room temperature.

Under the assumption, that every electron experiences the same average periodic potential V(r). Thus the Schrodinger equations describing the motion of each electron will be identical. The solution of equation (3.1) under mean-field approximation, the electronic Hamiltonian $\mathcal{H}_e$is given as

$$\mathcal{H}_e\Phi_n(\boldsymbol{r}) = \left(\sum_i \frac{p_i^2}{2m^*} + V(\boldsymbol{r})\right)\Phi_n(\boldsymbol{r}) = E_n\Phi_n(\boldsymbol{r}) \qquad (3.6)$$

Here, p_i is the electronic momentum and m^* is the effective mass of the electron, E_n is energy of an electron in an eigenstate labeled by n. The calculation of the electronic energies E_n includes the determination of the one-electron potential V(r) which can be calculated either from first principles with the atomic numbers and positions as the only input parameters or through simpler method, known as semi-empirical approaches, the potential is expressed in terms of parameters which are determined by fitting experimental results. Once the potential is known, it is still a complicated issue to solve equation (3.6). It is often convenient to utilize the symmetry

of the crystal to simplify this calculation. Here by "symmetry" we mean geometrical transformations which leave the crystal unchanged, refer to equation (3.4).

The one dimensional eigenfunction $\Phi_n(\boldsymbol{x})$ associated with a single electron can be expressed as a sum of Bloch functions:

$$\Phi(\boldsymbol{x}) = \sum_k A_k \, \Phi_k(\boldsymbol{r}) = \sum_k A_k \, u_k(x) e^{ikx} \qquad (3.7)$$

The plot of the electron energies in (3.6) versus k is known as the electronic band structure of the crystal.

For all the allowed possible values of wavevector k to vary is termed as the extended zone scheme with the condition i.e. both k and $k + {}^{2n\pi}/_{R}$ must satisfy equation (3.3) to maintain the consequence of the translation symmetry of the crystal. The k can also be replaced by;

$$k' = k - {}^{2n\pi}/_{R} \qquad (3.8)$$

where n is an integer chosen to limit k' to the interval $[-{}^{\pi}/_{R}, {}^{\pi}/_{R}]$ in k-space and known as the first Brillouin zone. The full band structure resulting from restricting the wave vector k to the first Brillouin zone is known as the reduced zone scheme. In this scheme the wave functions are indexed by an integer n (known as the band index) and a wave vector k restricted to the first Brillouin zone.

Also, the principal points to recall are that an electron feels the same potential at r and r', if

$$\boldsymbol{r'} = \boldsymbol{r} + \boldsymbol{R_l} \qquad (3.9)$$

where $\boldsymbol{R_l} = \boldsymbol{l_i a_i}$ is a lattice vector, and the a_i's are the minimum translation vectors (l_i are integers and we sum over repeated indices). The primitive or "minimum volume" unit cell has a volume $\Omega_c = |\boldsymbol{a_1} \cdot \boldsymbol{a_2} \times \boldsymbol{a_3}|$. The corresponding reciprocal lattice can be generated by the reciprocal lattice vectors, $\boldsymbol{G_m} = m_i \boldsymbol{b_i}$, where m_i are integers and the b_i are obtained from

$$\boldsymbol{b_i} = 2\pi \frac{\boldsymbol{a_j} \times \boldsymbol{a_k}}{|\boldsymbol{a_1} \cdot \boldsymbol{a_2} \times \boldsymbol{a_3}|} \qquad (3.10)$$

3.2.1 Diamond & Zinc blende structures

Let consider the Fig. 1 the face centered cubic (FCC) lattice whose base vectors are given by: $a_1 = \left(0, \frac{1}{2}, \frac{1}{2}\right) a_0$, $a_2 = \left(\frac{1}{2}, 0, \frac{1}{2}\right) a_0$, and $a_3 = \left(\frac{1}{2}, \frac{1}{2}, 0\right) a_0$, where a_0 is the side of the lattice. The zinc blende structure is formed from this face-centered cubic lattice by placing at each site of the lattice an elementary pattern composed of an atom of zinc and an atom of sulphur separated by a distance equal to one quarter of the diagonal of the unit cell (see Fig. 1).

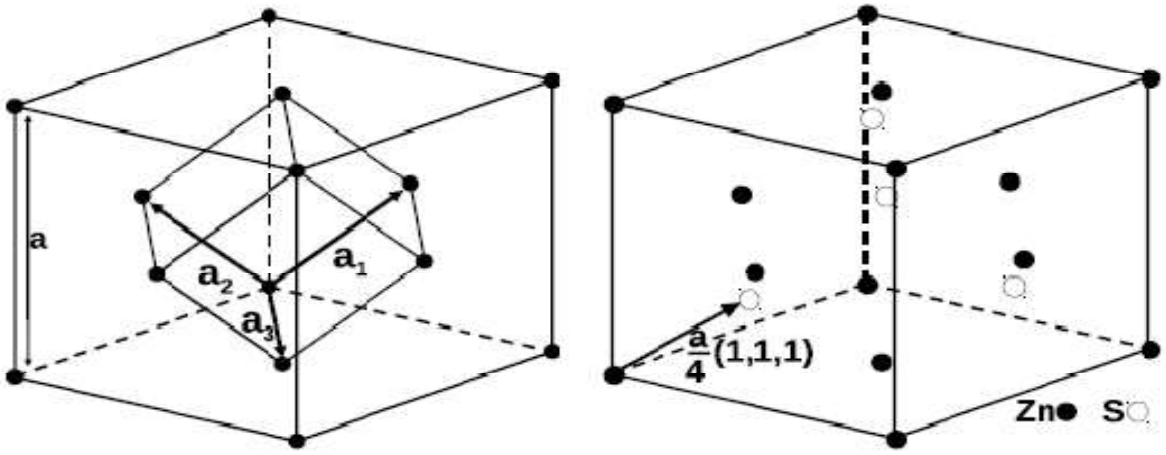

Figure 1. Face-centered cubic structure (left) and zinc blende lattice (right)

The reciprocal lattice of a face-centered cubic lattice, and as a consequence for a zinc blende structure, is a centered cubic lattice whose base vectors are given by $\boldsymbol{b_1} = \frac{2\pi}{a_0}(-1,1,1)$, $\boldsymbol{b_1} = \frac{2\pi}{a_0}(1,-1,1)$, $\boldsymbol{b_1} = \frac{2\pi}{a_0}(1,1,-1)$. Considering the high symmetry of the Brillouin zone, the band structure calculations can be considerably reduced using the symmetry operations of the crystal. It can be easily proved that a reduced region representing 1/48th of the Brillouin zone is sufficient to determine the energetic structure of the zinc blende crystals. The reduced region is delimited by the following points whose coordinates are given in units of (2π/a): Γ = (0, 0, 0), X = (0, 1, 0), K = (0.75, 0.75, 0), L = (0.5, 0.5, 0.5), and U = (0.25, 1, 0.25) (Fig. 2).

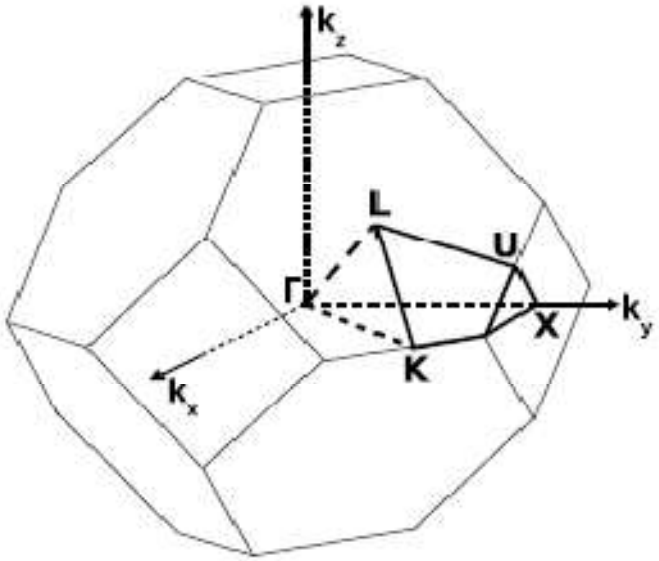

Figure 2. Brillouin zones of the zincblende

A vector $\boldsymbol{g} = \boldsymbol{lb_1} + \boldsymbol{mb_2} + \boldsymbol{nb_3}$ of the reciprocal lattice can be expressed as:

$$\boldsymbol{g} = \frac{2\pi}{a_0}[(-l+m+n)\boldsymbol{a_1} + (l-m+n)\boldsymbol{a_2} + (l+m-n)\boldsymbol{a_3}] \quad (3.11)$$

Its norm is then given by:

$$|\boldsymbol{g}|^2 = \left(\frac{2\pi}{a_0}\right)^2 [(3l^2 + 3m^2 + 3n^2 - 2lm - 2mn - 2ln)] \quad (3.12)$$

Therefore, the groups of symmetrical vectors refer to Fig.2 of the zincblende structure are (coordinates are in units of 2π/a) inbuilt in TNL-FB simulator:

- $g_0 = (0,0,0)$ (the origin)
- $g_3 = (-1,-1,-1), (\pm 1,0,0), (0,\pm 1,0), (0,0,\pm 1), (1,1,1)$
- g_4 =(−1, −1, 0), (−1, 0, −1), (0, −1, −1), (0, 1, 1), (1, 0, 1), (1, 1, 0)
- $g_8 = (-2,-1,-1), (-1,-2,-1), (-1,-1,-2), (-1,0,1), (-1,1,0), (0,-1,1),$ $(0,1,-1), (1,-1,0), (1,0,-1), (1,1,2), (1,2,1), (2,1,1)$
- $g_{11} = (-2,-2,-1), (-2,-1,-2), (-2,-1,0), (-2,0,-1), (-1,-2,-2), (-1,-2,0),$ $(-1,-1,1), (-1,0,-2), (-1,1,-1), (-1,1,1), (0,-2,-1), (0,-1,-2), (0,1,2),$

$(0, 2, 1), (1, -1, -1), (1, -1, 1), (1, 0, 2), (1, 1, -1), (1, 2, 0), (1, 2, 2), (2, 0, 1),$

$(2, 1, 0), (2, 1, 2), (2, 2, 1)$

- g_{12} =(−2, −2, −2), (±2, 0, 0), (0, ±2, 0), (0, 0, ±2), (2, 2, 2) . . .

We can neglect pseudopotential form factors with $|\boldsymbol{g}|^{\mathbf{2}} = \left(\frac{2\pi}{a_0}\right)^2$ because typically Vg decreases as g^{-2} for large g. Therefore, only 6 pseudopotential form factors are sufficient for the calculation.

3.2.2 Wurtzite structure

The wurzite structure is shown in Fig. 3. The base vectors of the hexagonal lattice are shown in the left panel of Fig. 7: $\boldsymbol{a_1} = (\mathbf{1},\mathbf{0},\mathbf{0})\boldsymbol{a_0}$, $\boldsymbol{a_2} = \left(\mathbf{1},\sqrt{\mathbf{3}},\mathbf{0},\right)\frac{\boldsymbol{a_0}}{\mathbf{2}}$, **and** $\boldsymbol{a_3} = (\mathbf{0},\mathbf{0},\boldsymbol{c})$. The compact hexagonal structure is made from the hexagonal lattice by placing at each site of the lattice two atoms separated by a vector $\boldsymbol{\tau} = \frac{\mathbf{1}}{\mathbf{3}}\boldsymbol{a_1} + \frac{\mathbf{1}}{\mathbf{3}}\boldsymbol{a_2} + \frac{\mathbf{1}}{\mathbf{2}}\boldsymbol{a_1}$ (see middle panel of figure 7). Finally, the wurtzite structure is made from the compact hexagonal lattice by placing at each site two atoms separated by a vector ua3, where $u \approx 0.375$ is a parameter relative to the wurtzite structure (right panel of figure 7). Therefore, as a result, the elementary pattern of the wurtzite structure is made of 4 atoms.

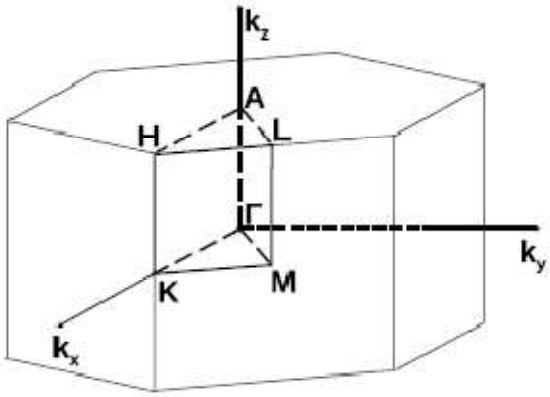

Figure 3. Wurtzite structure

The reciprocal lattice of the hexagonal lattice is also hexagonal. The base vectors of this reciprocal lattice are given by $\boldsymbol{b_1} = \frac{2\pi}{a_0\sqrt{3}}\left(\sqrt{3},1,0\right)$, $\boldsymbol{b_1} = \frac{4\pi}{a_0\sqrt{3}}(0,1,0)$, and $\boldsymbol{b_1} = \frac{2\pi}{c}(0,0,1)$. Thus, the first Brillouin zone of the reciprocal lattice of the hexagonal structure is also hexagonal. Given the high symmetry of the

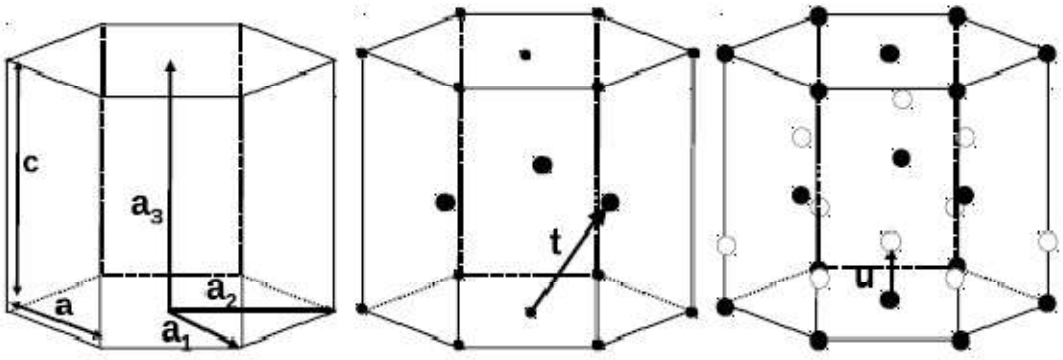

Figure 4. Hexagonal lattice (left), compact hexagonal structure (middle) and wurtzite structure (right).

Brillouin zone, the band structure calculations can be considerably reduced using the symmetry operations of the crystal. In particular, it can easily be proved that a reduced region representing 1/24th of the Brillouin zone such as reported in the Fig. 3 is sufficient to determine the energetic structure of the wurtzite crystals.

This reduced region is delimited by the following points:

Γ = (0, 0, 0) (origin),

H = (2π/3a , 2π/a , 2π/c) (extremity of an edge joining two rectangular sides),

A = (0, 0, π/c) (center of an hexagonal side),

K = (2π/3a , 2π/a , 0) (middle of an edge joining two rectangular sides),

L = (0, 2π/a , 2π/c) (middle of an edge joining an hexagonal and a rectangular side), and

M = (0, 2π/a , 0) (center of a rectangular side).

The reciprocal lattice vector of wurtzite structure can be expressed as:

$$\boldsymbol{g} = l\boldsymbol{i} + \frac{2m-l}{\sqrt{3}}\boldsymbol{j} + \sqrt{\frac{3}{8}}\boldsymbol{k} \tag{3.13}$$

Its norm is then given by:

$$|\boldsymbol{g}|^2 = \left(\frac{2\pi}{a_0}\right)^2 \left[\frac{4}{3}(l^2 + m^2 - lm) + \frac{3}{8}n^2\right] \tag{3.14}$$

Therefore, the reciprocal lattice vectors in increasing order of the modulus are in units of (2π/a):
Therefore, the groups of vectors of the zincblende structure are (coordinates are in units of 2π/a):

- $g_0 = (0, 0, 0)$ (the origin)
- $g_{\frac{3}{8}} = (0, 0, \pm 1)$
- $g_{1+\frac{1}{3}} = (-1, -1, 0), (-1, 0, 0), (0, -1, 0), (0, 1, 0), (1, 0, 0), (1, 1, 0)$
- $g_{1+\frac{1}{2}} = (0, 0, \pm 2)$
- $g_{1+\frac{17}{24}} = (\pm 1, 0, \pm 1), (0, \pm 1, \pm 1), (-1, -1, -1), (1, 1, 1), (-1, -1, 1), (1, 1, -1)$
- $g_{2+\frac{5}{6}} = (0, \pm 1, \pm 2), (\pm 1, 0, \pm 2), (-1, -1, -2), (1, 1, 2), (-1, -1, 2), (1, 1, -2)$
- $g_{3+\frac{3}{8}} = (0, 0, \pm 3)$
- $g_4 = (1, 2, 0), (-1, -2, 0), (2, 1, 0), (-2, -1, 0), (-1, 1, 0), (1, -1, 0)$

- $g_{4+\frac{3}{8}} = (1,-1,\pm1),(-1,1,\pm1),(1,2,\pm1),(-1,-2,\pm1),(2,1,\pm1),(-2,-1,\pm1)$
- $g_{4+\frac{17}{24}} = (0,\pm1,\pm3),(\pm1,0,\pm3),(-1,-1,-3),(1,1,3),(-1,-1,3),(1,1,-3)$
- $g_{5+\frac{1}{3}} = (\pm2,0,0),(0,\pm2,0),(2,2,0),(2,2,0)$
- $g_{5+\frac{1}{2}} = (1,-1,\pm2),(-1,1,\pm2),(2,1,\pm2),(1,2,\pm2),(-2,-1,\pm2),(-1,-2,\pm2)$
- $g_{5+\frac{17}{24}} = (\pm2,0,\pm1),(0,\pm2,\pm1),(2,2,1),(-2,-2,1),(2,2,-1),(-2,-2,-1)$
- $g_{6} = (0,0,\pm4)$
- $g_{6+\frac{5}{6}} = (\pm0,\pm2,\pm2),(\pm2,\pm0,\pm2),(2,2,2),(-2,-2,2),(2,2,-2),(-2,-2,-2)$
- $g_{7+\frac{1}{3}} = (\pm1,\pm0,\pm4),(\pm0,\pm1,\pm4),(-1,-1,-3),(1,1,3),(-1,-1,3),(1,1,-3)$
- $g_{7+\frac{3}{8}} = (-1,1,\pm3),(1,-1,\pm3),(2,1,\pm3),(1,2,\pm3),(-2,-1,\pm3),(-1,-2,\pm3)\ldots$

The reciprocal lattice vectors with $|\boldsymbol{g}|^2 > \left(\mathbf{7}+\frac{\mathbf{1}}{\mathbf{3}}\right)\left(\frac{2\pi}{a_0}\right)^2$ can be neglected for calculation of the pseudopotential form factors.

3.3 Basic Theroy for Electronic Bands

The symmetric eigenfunctions is used to the understanding of the evolution of the bandstructure and the energy eigenvalues are used to extract the information of the individual atoms in particular state that constitutes the semiconductor crystal. Most of the semiconductors have tetrahedral bonding with sp^3 hybridization. However, the individual atoms have the outermost (valence) electrons in s- and p-type orbitals. The symmetry (or geometric) properties of these orbitals are made most clear by looking at their angular parts

$$\begin{aligned} s &= 1 \\ p_x &= \frac{x}{r} = \sqrt{3}\sin\theta\cos\varphi \\ p_y &= \frac{y}{r} = \sqrt{3}\sin\theta\sin\varphi \\ p_z &= \frac{z}{r} = \sqrt{3}\cos\theta \end{aligned} \tag{3.15}$$

The band structure with gaps and allowed bands is created by crystal itself. It turns out that the states near the band-edges behave very much like the s-type and the three p-type (p_x, p_y and p_z) states that they had when they were individual atoms. Electronic band structure simulation methods can be classified into two general categories [1].

3.3.1 AB-initio methods, Hartree-Fock or Density Functional Theory (DFT)

DFT theory simulates the electronic structure exploiting first principles, without using empirical fitting parameters. A variational approach is utilized for calculation of the ground state energy associated with many-body system, where the system is defined at the atomic level. The DFT method is capable to predict electronic band structure, however the DFT based methods suffer with expensive computation burdens and requires massively parallel computers.

3.3.2 E*mpirical* methods

Empirical methods can be classified into four types of different approaches for the prediction of full electronic band structures through simulation.

a. Orthogonalized Plane Wave (OPW) [2],
b. Tight-Binding (Linear Combination of Atomic Orbitals (LCAO)) method [3],
c. k. p method [4],
d. Local or non-local empirical pseudopotential method (EPM) [5]-[6].

All above mentioned methods use empirical parameters to fit experimental data. The empirical methods are computationally less expensive compared to ab initio methods. The empirical pseudopotential method (EPM) provides a relatively easy means for simulating the electronic band structure.

3.4 The Empirical Pseudopotential Method

In pseudopotential method, the crystal wave funtion $\psi_{\mathbf{k}}$ is chosen such that it remains orthogonal to the core states. This is done by expanding $\psi_{\mathbf{k}}$ as a smooth part of combinations of symmetric Bloch functions $\varphi_{\mathbf{k}}$, augmented with a linear combination of core states. This is given as

$$\psi_{\mathbf{k}} = \varphi_{\mathbf{k}} + \sum_{t} b_{\mathbf{k},t}\Phi_{\mathbf{k},t} \tag{3.16}$$

Here $b_{\mathbf{k},t}$ represents orthogonalization coefficients and $\Phi_{\mathbf{k},t}$ are core wave functions. For Si-14, the summation over t in Eq. (3.16) is a sum over the core states $1s^2\ 2s^2\ 2p^6$. Since the crystal wave function is constructed to be orthogonal to the core wave functions, the orthogonalization coefficients can be calculated, thus yielding the final expression

$$\psi_{\mathbf{k}} = \varphi_{\mathbf{k}} - \sum_{t} \langle \Phi_{\mathbf{k},t} | \varphi_{\mathbf{k}} \rangle \Phi_{\mathbf{k},t} \ . \tag{3.17}$$

The wave functions and energies of electrons in a crystal are given by solving the Schrodinger equation

$$H\psi_{n,k} = E_n(\vec{k})\psi_{n,k}(\vec{r}) \tag{3.18}$$

where, H is the Hamiltonian of the System, $\psi_{n,k}$ is the wave functions, $E_n(\vec{k})$ the corresponding eigenvalues, $\vec{k}$ the wave vectors of the wave functions, and n is the band index.

For the large number of electrons involved even in small clusters, exact solution of this equation is computationally unfeasible. Several approximations are used to convert this problem into one which can be solved in a reasonable amount of time.

The Born Oppenheimer approximation is inbuilt in TNL-FB simulator for the simulation of full electronic band structures using pseudopotential method:

- Core electrons, assumed to be attached to the atomic cores, only the valence electrons are free to move.
- The cores are fixed in position (the Born-Oppenheimer approximation).

- Each valence electron moves in the mean field of the fixed cores and the other valence electrons.

These assumptions give rice to the effective Hamiltonian

$$H = -\frac{h^2}{2m}\Delta^2 + V_P(\vec{r}) \tag{3.19}$$

$V_P(\vec{r})$ is pseudopotential, and is determined by using empirical pseudopotential method (EPM). The total pseudopotential experienced by electron includes contribution of two pseudopotential components i.e. local and nonlocal pseudopotential and is given as

$$V_P(\vec{r}) = V_L(\vec{r}) + \sum_{l=0}^{\infty} \Pi_l^{+} A_l(E) f_l(\vec{r}) \Pi_l \tag{3.20}$$

Here the first term V_L depicts local part, while V_{NL} represent the nonlocal part and Π_l is the projection operator for angular momentum states l and $A_l(E)$ is the energy dependent well depth.

3.4.1 Nonlocal pseudopotentials

The local part of the pseudopotential ($V_L(\vec{r})$) is found capable to predict accurately the gross features of the band structures correctly. However, the consideration and contribution of the nonlocal pseudopotential can provide much more accuracy over a broad range of energy scales. The calculated band widths and band dispersion are observed much closer to the experimental values with the nonlocal calculations as compared to the local calculations. The incorporation of the correct angular momentum dependence in nonlocal calculations are also much more satisfactory and justify the nature of the potential experienced by the valence electrons. In the plane wave basis the matrix elements of the nonlocal pseudopotential is given as

$$V_{NL}(\vec{G},\vec{G}') = \frac{4\Pi}{\Omega_a}\sum_{l,i} A_l^i(E) P_l(cos(\theta_{G,G'}))S'(\vec{G}-\vec{G}')F_l^i(\vec{G},\vec{G}') \quad (3.21)$$

Here, P_l represents the angular momentum of electrons, G are reciprocal lattice vector, Ω_a is the volume.

3.4.2 Spin Orbit coupling in Band Theory

The orbital angular momentum (l) and electron spin (s) in light elements are good quantum numbers. The magnetic field generated in these elements by the orbiting electron is too weak. It cannot induce coupling with the electron spin. However, in heavier elements the nearly relativistic speed of the valence electron produces a sufficiently large magnetic field that l and s are coupled, giving rise to $j = l + s$ as the good quantum number. The spin-orbit interaction thus couples electron dynamics in spin and ordinary spaces, thereby reducing the overall symmetry of the Hamiltonian. This relativistic effect is represented by the operator,

$$H_{so} = \frac{h}{4m^2c^2}\vec{\sigma}.(\nabla\vec{v}_P \times \vec{p}) \tag{3.22}$$

where $\vec{\sigma}$ are the pauli spin matrices, $\vec{V}_P$is the pseudopotential, $\vec{p}$ is the electron momentum, m is the electron effective mass, and c is the speed of light. The matrix elements of the new Hamiltonian in the plane wave representation are given by

$$\begin{aligned} <\vec{k}+\vec{G}',s'|H|\vec{k}+\vec{G},s> = \frac{\hbar^2}{2m}|\vec{k}+\vec{G}|^2\delta_{\vec{G},\vec{G}}\delta_{s,s'} + S_S(\vec{G}-\vec{G}')[V_S(|\vec{G}-\vec{G}'|^2)\delta_{S,S'} - \\ i\lambda_S(\vec{G}'\times\vec{G}).\delta_{S,S'}] + iS_A(\vec{G}-\vec{G}')[V_A(|\vec{G}-\vec{G}'|^2)\delta_{S,S'} - \\ i\lambda_S(\vec{G}'\times\vec{G}).\delta_{S,S'}] \end{aligned} \tag{3.23}$$

For a binary semiconductor consisting of two types of atoms ($A \neq B$), we define

$$\lambda_S = \frac{1}{2}(\lambda_1 + \lambda_2) \tag{3.24}$$

$$\lambda_A = \frac{1}{2}(\lambda_1 - \lambda_2) \tag{3.25}$$

Where

$$\lambda_1 = \mu B_{nl}^A(G)B_{nl}^A(G') \tag{3.26}$$

$$\lambda_2 = a\mu B_{nl}^B(G)B_{nl}^B(G') \tag{3.27}$$

Where μ is the adjustable parameter chosen in order to obtain the aplitting Δ of the valence Band at Γ correctly, and a is the ratio of the contribution from atom A to the contribution from atom B at Γ. The B_{nl} are defined as

$$B_{nl}(G) = C\int_0^\infty r^2\, R_{nl}(r)j_l(G)dr \tag{3.27}$$

where j_l are the spherical Bessel functions, C is determined by the condition

$$Lim_{G\to 0}\frac{B_{nl}(G)}{G} = 1 \tag{3.28}$$

And R_{nl} are the radial parts of the outermost electron wave functions.

3.4.3. Local Pseudopotential

In the TNL-FB (Full Band) simulator, the local pseudopotential is included as

$$V_P(\vec{r}) = \sum_{R.j} \upsilon_j (\vec{r} - \vec{R} - \vec{d}_j) \tag{3.29}$$

where $\vec{R}$ is the position of a lattice site, d_j is the position of the j^{th} basis atom with respect to the lattice site, and v_j is the atomic pseudopotential of the j th basis atom.

The sum is taken over all lattice sites and basis atoms. Fourier expansion of υ_j gives

$$v_j(\vec{r} - \vec{R} - d_j) = \frac{1}{Nn_a}\sum_G v_j\left(\vec{G}\right)\exp[i\vec{G}.(\vec{r} - \vec{R} - \vec{d}_j)] \tag{3.30}$$

where $\vec{G}$ are the reciprocal lattice vectors, N is the number of unit cells, n_a the number of basis atoms per unit cell, and the form factor

$$v_j(\vec{G}) = \frac{n_a}{\Omega_0} \tag{3.31}$$

where Ω_0 is the volume of the unit cell. There is a condition $v_j^*(\vec{G}) = v_j(-\vec{G})$ on $v_j(\vec{G})$ to ensure that $v_j(\vec{r})$ is real If the atomic potential$v_j(\vec{r}) = v_j(|\vec{r}\,|)$, as we might expect for a spherically symmetric atom,

$$v_j\left(\vec{G}\right) = v_j\left(\left|\vec{G}\right|\right) = \frac{4\pi n_\alpha}{\Omega_0}\int r^2 j_0(Gr)v_j(r)dr \tag{3.32}$$

where j_0 is the zeroth order spherical Bessel function. That is, for symmetric atomic potentials, the form factors $\upsilon_j(\vec{G})$ depend on the magnitude of $(\vec{G})$ only. Substitution of Equation (3.7) into Equation (3.6) gives

$$V_P(\vec{r}) = \frac{1}{Nn_a}\sum_G \sum_{R.j} v_j\left(\vec{G}\right)\exp[i\vec{G}.(\vec{r} - \vec{R} - \vec{d}_j)] \tag{3.33}$$

For the structures under consideration, the second summation over $\vec{R}$ and j can be carried out separately, leaving $V_p(\vec{r})$ as a closed form function of $v_j(\vec{G})$ only. The factors $v_j(\vec{G})$ are determined empirically from optical data giving known energies in the band structure.

3.4 The diamond structure Pseudopotential

The diamond lattice is composed of two interpenetrating fcc lattices displaced from one another by $\left(\frac{1}{4},\frac{1}{4},\frac{1}{4}\right)a_0$. If the origin is taken half way between the two fcc lattices, then $f = \pm\left(\frac{1}{8},\frac{1}{8},\frac{1}{8}\right)a_0$ where a_0 is the lattice constant. Hence we take $n_a = 2$ and $\vec{d}_1 = -\vec{d}_2 = -\vec{f}_1$. Since the two atoms are of the same type $v_1 = v_2$. The Equation (3.33) can be written as

$$V_P(\vec{r}) = \frac{1}{2N}\sum_G v_1\left(\vec{G}\right)\exp(i\vec{G}.\vec{r})\sum_R \exp\left(-i\vec{G}.\vec{R}\right)\sum_j \exp\left(-i\vec{G}.\vec{d}_j\right) \tag{3.34}$$

Here $\vec{G}.\vec{R} = 2n\pi$ by definition, so

$$\sum_R \exp\left(-i\vec{G}.\vec{R}\right) = \sum_R 1 = N \tag{3.35}$$

and

$$\begin{aligned} V_P(\vec{r}) &= \sum_G \upsilon_1\left(\vec{G}\right)\exp\left(i\vec{G}.\vec{r}\right)\frac{1}{2}\left[\exp\left(i\vec{G}.\vec{t}_1\right)+\exp\left(-i\vec{G}.\vec{t}_1\right)\right] \\ &= \sum_G \upsilon_1\left(\vec{G}\right)\exp\left(i\vec{G}.\vec{r}\right)\cos\left(\vec{G}.\vec{t}_1\right) \\ &= \sum_G \upsilon_1\left(\vec{G}\right)\mathrm{S}\left(\vec{G}\right)\exp(i\vec{G}.\vec{r}) \end{aligned} \tag{3.36}$$

where

$$S(\vec{G}) = \cos(\vec{G}.\vec{t}_1) \tag{3.37}$$

3.5 The zinc-blende structure Pseudopotential

The zinc-blende structure is similar to the diamond structure but with two different basis atoms, here $v_1 \neq v_2$. From Equation (3.33) using Equation (3.35) we have

$$V_P(\vec{r}) = \frac{1}{n_a}\sum_G \exp(i\vec{G}.\vec{r}) \sum_j v_j (\mathrm{G})\exp(-i\vec{G}.\vec{d}_j) \tag{3.38}$$

$$V_P(\vec{r}) = \sum_G \exp(i\vec{G}.\vec{r}) \frac{1}{2}[\upsilon_1(\vec{\mathrm{G}})\exp(i\vec{G}.\vec{t}_1) + \upsilon_2(\vec{\mathrm{G}})\exp(-i\vec{G}.\vec{t}_2)] \tag{3.39}$$

Using $\exp(i\theta) = \cos(\theta) + i\sin(\theta)$ and collecting terms in $\cos(\vec{G}.\vec{t}_1)$ and $\sin(\vec{G}.\vec{t}_1)$ we obtain

$$\begin{aligned} V_P(\vec{r}) &= \sum_G \exp(i\vec{G}.\vec{r})[V_S(G)\cos(\vec{G}.\vec{t}_1) + iV_A(G)\sin(\vec{G}.\vec{t}_1)] \\ &= \sum_G \exp(i\vec{G}.\vec{r})[V_S(G)S_S(G) + iV_A(G)S_A(G)] \end{aligned} \tag{3.40}$$

where

$$\begin{aligned} V_S(G) &= \frac{1}{2}[\upsilon_1(G) + \upsilon_2(G)] \\ V_A(G) &= \frac{1}{2}[\upsilon_1(G) - \upsilon_2(G)] \end{aligned} \tag{3.41}$$

and

$$\begin{aligned} S_S(\vec{G}) &= \cos(\vec{G}.\vec{t}_1) \\ S_A(\vec{G}) &= \sin(\vec{G}.\vec{t}_1) \end{aligned} \tag{3.42}$$

For computational purposes, it is useful to define $\vec{G}$ in units of $2\pi/a_0$

$$\vec{G} = \frac{2\pi}{a_0}(G_x, G_y, G_z) \tag{3.43}$$

from which, by Equation (3.30), we obtain

$$\begin{aligned} S_S(\vec{G}) &= \cos[\frac{\pi}{4}(G_x + G_y + G_z)] \\ S_A(\vec{G}) &= \sin[\frac{\pi}{4}(G_x + G_y + G_z)] \end{aligned} \tag{3.44}$$

3.6 The hexagonal structure Pseudopotential

In the hexagonal structure there are four basis atoms of two different types on each lattice. The structure is characterized by three lengths a_0 , c_0 and v_0. If we assume perfect packing then

$$c_0/a_0 = \sqrt{8+3}, u_0 = 0.375 \tag{3.45}$$

The primitive lattice translation vectors are

$$\begin{aligned} \vec{a}_1 &= \left(\tfrac{\sqrt{3}}{2}, -\tfrac{1}{2}, 0\right) a_0 \\ \vec{a}_2 &= (0,1,0) a_0 \\ \vec{a}_3 &= \left(0,0,\tfrac{c_0}{a_0}\right) a_0 \end{aligned} \tag{3.46}$$

and basis atom positions are

$$\begin{aligned} \vec{d}_1 &= \left(-\frac{1}{4\sqrt{3}}, -\frac{1}{12}, -\frac{1-2u_0}{\sqrt{6}}\right) a_0 = -\vec{d}_4 \\ \vec{d}_2 &= \left(-\tfrac{1}{4\sqrt{3}}, -\tfrac{1}{12}, -\tfrac{1+2u_0}{\sqrt{6}}\right) a_0 = -\vec{d}_3 \end{aligned} \tag{3.47}$$

where atoms 1 and 3, and 2 and 4 are indentical. So from Equation (3.33) and (3.35) we have

$$V_P(\vec{r}) = \textstyle\sum_G \exp(-\vec{G}.\vec{r}) \frac{1}{4} \{\upsilon_1(\vec{G})[\exp(i\vec{G}.\vec{d}_2) + \exp(-i\vec{G}.\vec{d}_1)] + \{\upsilon_2(\vec{G})[\exp(i\vec{G}.\vec{d}_1) + \exp(-i\vec{G}.\vec{d}_2)]\} \tag{3.48}$$

If we write υ_1 and υ_2 in terms of V_S and V_A, after some trigonometric manipulation we obtain

$$\begin{aligned} V_P(\vec{r}) = \sum_G \exp(-\vec{G}.\vec{r}) [V_S(\vec{G}) \cos\left(\frac{\vec{d}_1+\vec{d}_2}{2}\right) \cos\left(\frac{\vec{d}_1+\vec{d}_2}{2}\right) \\ + i V_A(\vec{G}) \cos\left(\tfrac{\vec{d}_1+\vec{d}_2}{2}\right) \sin\left(\tfrac{\vec{d}_1+\vec{d}_2}{2}\right)] \end{aligned} \tag{3.49}$$

By Assuming a hard sphere packing, we can relate the lattice constant in the zincblende and hexagonal forms by

$$a_0(ZB) = \sqrt{2} a_0(hex) \tag{3.50}$$

and by analogy with Equation (3.43) we define

$$\vec{G} = \frac{\sqrt{2}\pi}{a_0(hex)} (G_x, G_y, G_z) \tag{3.51}$$

From Equations (3.47), (3.49) and (3.41) we obtain Equation (3.40) again, but with

$$S_S(\vec{G}) = \cos((\vec{G}.\vec{t}) \cos(2\pi u_0 G_z/\sqrt{3})$$
$$S_A(\vec{G}) = \cos((\vec{G}.\vec{t}) \sin(2\pi u_0 G_z/\sqrt{3}) \quad (3.52)$$

where $\vec{t} = (1/\sqrt{48},\ 1/12, 1/\sqrt{6})$.

3.5 TNL Material Database inbuilt in TNL-FB Simulator

Various material database associated with the binary semiconductors structures (diamond & zincblende and wurtzite structures) for the simulation of full electronic band structure are inbuilt in TNL material database.

3.5.1 Lattice constants of Diamond and Zincblende structure semiconductors

	Crystal	a [^{o}A]
Diamond	Si	5.43
	Ge	5.65
	C	3.567
Zinc-blende	GaP	5.45
	GaAs	5.653
	GaSb	6.1
	InP	5.86
	InAs	6.0583
	InSb	6.479
	GaN	4.52
	AlN	3.11
	AlAs	5.661
	InN	4.98
	HgTe	6.454
	CdTe	6.486
	AlSb	6.1355
	AlP	5.4635
	GaP	5.45

The lattice parameters of the diamond and zincblende structure ternary semiconductors can be interpolated by using binary semiconductors lattice parameters. The direct input of the lattice parameters of binary, ternary and quaternary semiconductors which are obtained through XRD studies can be directly inputted in the TNL-FB simulator.

Users have flexibilities to use other zincblende materials which are not in the TNL database by inputting the lattice parameters and symmetric and asymmetric pseudopotentials.

3.5.2 Lattice constants of Wurtzite structure semiconductors

Crystal	a [^{o}A]	c [^{o}A]	u
GaN	-0.292	-0.599	-0.181
AlN	-0.499	-0.5	-0.289
InN	-0.255	-0.228	-0.217
ZnS	-0.22	-0.24	-0.19
CdS	-0.24	-0.26	-0.2
CdSe	-0.23	-0.25	-0.2
ZnO	-0.33	-0.42	-0.27

Here, a & c is the lattice parameters and u is the internal structure factor depends upon a & c. The lattice parameters of the wurtzite structure ternary semiconductors can be interpolated by using binary semiconductors lattice parameters. The direct input of the lattice parameters of binary, ternary and quaternary semiconductors which are obtained through XRD studies can be directly inputted in the TNL-FB simulator.

Users have flexibilities to use other zincblende materials which are not in the TNL database by inputting the lattice parameters and symmetric and asymmetric pseudopotentials.

3.5.3 Pseudopotential form factors

The inbuilt pseudopotential form factors of ternary semiconductors can be interpolated by using binary semiconductors symmetric and asymmetric form factors. Users have flexibilities to use other semiconductors which are not in the TNL database by inputting the lattice parameters and symmetric and asymmetric pseudopotentials.

Reciprocal lattice vectors G for zinc-blende structure semiconductors and pseudopotential form factors V_S and V_A in Ry at various high symmetry points on the lattice.

G	**111**		**200**		**210**		**212**	
G^2	**3**		**4**		**8**		**11**	
	VS	**VA**	**VS**	**VA**	**VS**	**VA**	**VS**	**VA**
Si*	-0.224	0	0	0	0.055	0	0.072	0
Ge	-0.221	0	0	0	0.019	0	0.056	0
GaP	-0.23	0.119	0	0.07	0.02	0	0.057	0.0025
GaAs	-0.236	0.08	0	0.049	0.015	0	0.053	0.0075
GaSb	-0.2043	0.018	0	0.0452	0.0076	0	0.04805	0.004
InP	-0.2	0.0965	0	0.0804	0.00269	0	0.0492	0.00255
InAs	-0.209	0.053	0	0.0445	0	0	0.0442	0.0085
InSb	-0.119	0.09893	0	0.064	-0.0125	0	0.03985	0.0078
GaN	-0.222	0.338	0	0.17	0.018	0	0.0989	0.0192
AlN	-0.3192	0.77	0	0.32	0.08	0	0.23	0.016
AlAs	-0.21	0.104	0	0.06	0.023	0	0.0688	0.005
InN	-0.1722	0.23874	0	0.2321	-0.0055	0	0.0946	0.03149
HgTe	-0.23	-0.095	0	-0.08	-0.025	0	0.03	-0.03
CdTe	-0.2	0.129	0	0.09	0	0	0.04	0.04
AlSb	-0.2256	0.007109	0	0.05896	0.028086	0	0.06333	0.004544
AlP	0.24131	0.030061	0	0.116	0.021262	0	0.249336	0.232543

Reciprocal lattice vectors G for wurtzite structure semiconductors and pseudopotential form factors V_S and V_A in Ry at various high symmetry points on the lattice.

Binary Group III-Nitrides

G	G^2	GaN		AlN		InN	
		Vs	Va	Vs	Va	Vs	Va
100	2.666	-0.599	0	-0.5	0.2	-0.228	0
002	3	-0.292	0.254	-0.499	0.115	-0.255	0.251
101	3.416	-0.181	0.2482	-0.289	0.2785	-0.217	0.274
102	5.666	-0.1499	0.23	-0.2	0	-0.01	0.109
210	8	0.029	0.1	0.1	0.2	0.044	0
103	9.4166	0.0587	0.03956	0.199	0	0.056	-0.032
200	10.666	0.031	0.2	0.009	0	0.025	0
212	11	0.066	0.04	0.1	0.2	0.015	0.029
201	11.416	0.05	0.006	0.3	0.0216	0.036	0.0205
004	12	0.1	0.001	0.2	0.004	0	0.0125
202	13.666	0.447	0.4	0.21	0.5	-0.1	0.016

Binary Group II-Sulphides & Oxides

G	G^2	ZnS		CdS		CdSe		ZnO	
		Vs	Va	Vs	Va	Vs	Va	Vs	Va
100	2.666	-0.24	0	-0.26	0	-0.25	0	-0.42	0
002	3	-0.22	0.23	-0.24	0.23	-0.23	0.19	-0.33	0.32
101	3.416	-0.19	0.19	-0.2	0.18	-0.2	0.15	-0.27	0.24
102	5.666	-0.06	0.1	-0.03	0.08	-0.07	0.09	-0.04	0.13
210	8	0.03	0	0.03	0	0.01	0	0.05	0
103	9.4166	0.06	0.02	0.04	0.05	0.03	0.05	0.07	0.01
200	10.666	0.07	0	0.04	0	0.04	0	0.07	0
212	11	0.07	0.02	0.04	0.05	0.04	0.05	0.07	0.01
201	11.416	0.07	0.02	0.04	0.05	0.04	0.05	0.06	0.01
004	12	0	0.02	0	0.05	0	0.05	0	0.01
202	13.666	0.04	0.01	0.02	0.03	0.02	0.03	0.05	0.04

References

1. P. Y. Yu and M. Cardona, Fundamentals of Semiconductors, Springer-Verlag, Berlin, 1999.
2. C. Herring, Phys. Rev., 57 (1940) 1169.
3. D. J. Chadi and M. L. Cohen, Phys. Stat. Sol. (b), 68 (1975) 405.
4. J. Luttinger and W. Kohn, Phys. Rev., 97 (1955) 869.
5. M. L. Cohen and T. K. Bergstresser, Phys. Rev., 141 (1966) 789.
6. J. R. Chelikowsky and M. L. Cohen, Phys Rev. B, 14 (1976) 556.
7. E. Fermi, Nuovo Cimento, 11 (1934) 157.
8. H. J. Hellman, J. Chem. Phys., 3 (1935) 61.
9. J. C. Phillips and L. Kleinman, Phys. Rev., 116 (1959) 287.
10. J. R. Chelikowsky and M. L. Cohen, Phys Rev. B, 10 (1974) 12.
11. L. R. Saravia and D. Brust, Phys. Rev., 176 (1968) 915.
12. S. Gonzalez, Masters Thesis, Arizona State University, 2001.
13. J. R. Chelikowsky and M. L. Cohen, Phys. Rev. B, 10 (1974) 5059.
14. K. C. Padney and J. C. Phillips, Phys. Rev. B, 9 (1974) 1552.
15. D. Brust, Phys. Rev. B, 4 (1971) 3497.
16. A. Srivastava, A. Saxena, P. K. Saxena, F. K.Gupta, P. Shakya, P. Srivastava, M. Dixit, S.Gambhir, R. K. Shukla & A. Srivastava, *Scientific Reports* 10, 18706 (2020).
17. P. K. Saxena, A. Srivastava, A. Saxena, F. K.Gupta, P. Shakya, A. Srivastava, R. K.Shukla, Journal of Electronic Materials, 50(4), 2417 (2021).